Signal processing in Ultrasound Doppler and Color Flow Imaging

Hans Torp, Department of Circulation and Medical Imaging
NTNU, Trondheim, Norway

1.1 Introduction

This paper reveals methods for extracting information about the velocity field from the Doppler signal. We shall restrict the analysis to time-discrete processes, and use the notation

$$z(n); \qquad n = ...,-2,-1,0,1,2,... \tag{1}$$

where $z(n)$ is the complex sample at time $t=nT$. For the Fourier transform, we use capital letters

$$Z(\omega) = \sum_n z(n) e^{-i\omega n} \tag{2}$$

and the frequency parameter ω is in the range $(-\pi,\pi)$. For continuous wave Doppler, the sampling interval T can be chosen arbitrarily, whereas for pulsed wave Doppler the sampling interval T equals the inverse of the pulse repetition frequency. By using the Doppler shift frequency Equation (9.25), we get the following relation between the blood velocity v and the normalized angular frequency ω:

$$v = \frac{c}{2\omega_0 T}\omega \tag{3}$$

Here c is the speed of sound, T is the sampling interval, and ω_0 is angular transmitted frequency.

In Section 2 the general principles for parameter estimation in a complex Gaussian process is treated, and in particular, the estimate of the autocorrelation function and the power spectrum. Section 3 covers the application of power spectrum analysis to continuous and pulsed wave Doppler instruments, and some practical algorithms for spectrum analysis, including FFT and chirp-Z transform. Signal processing for two-dimensional Doppler color flow imaging is treated in Section 4 , including spectral moment estimation, color coding, and wall motion rejection. The last section presents some recently developed methods for resolving velocity ambiguity in pulsed wave Doppler and color flow imaging.

2 Parameter estimation in a complex Gaussian process

A. Properties of a complex Gaussian process

A complex number $z = x + iy$ is defined as a (zero mean) complex Gaussian variable if the real and imaginary parts are joint Gaussian with probability density function

$$p(z) = \frac{1}{2\pi\sigma^2} e^{-\frac{zz^*}{2\sigma^2}} = \frac{1}{2\pi\sigma^2} e^{-\frac{x^2+y^2}{2\sigma^2}} \tag{4}$$

Note that the real and imaginary parts are independent random variables, and have equal variance σ. A complex Gaussian vector $\boldsymbol{z} = (z_1,z_2,...,z_n)$ is defined by its probability density function

$$p(\mathbf{z}) = \frac{1}{(2\pi)^n |\mu|} e^{-\frac{1}{2}\mathbf{z}^T \mu^{-1} \mathbf{z}} \tag{5}$$

where the covariance matrix μ is given by

$$\mu_{i,j} = < z_i \ z_j^* > \tag{6}$$

and the vector z^T is the transposed and complex conjugate of z. Note that the expectation value $<z_i \ z_j> = 0$ for all i,j.

A signal z(t) with a continuous or discrete time parameter t is a complex Gaussian process if every random vector $(z(t_1),..., z(t_n))$ which is obtained by sampling the process at n points is a complex Gaussian vector. The number n is arbitrarily large. The process $z(t)$ is completely determined by its autocorrelation function, which is a complex valued function of two time parameters

$$R(t_1,t_2) = < z(t_1)\, z(t_2)^* > \tag{7}$$

Note that $R(t,t) = |z(t)|^2$ is real valued when $t_1 = t_2$. This quantity is the signal power of the process.

If the process is stationary, i.e the stochastic properties are invariant under time shifts, the autocorrelation is only dependent on the time difference $\tau = t_1 - t_2$. In this case the notation is simplified to

$$R(\tau) = < z(t+\tau)\, z(t)^* > \tag{8}$$

The power spectrum of a stationary process $z(t)$ is defined as the Fourier transform of the autocorrelation function

$$G(\omega) = \int d\tau R(\tau) e^{i\omega\tau} \tag{9}$$

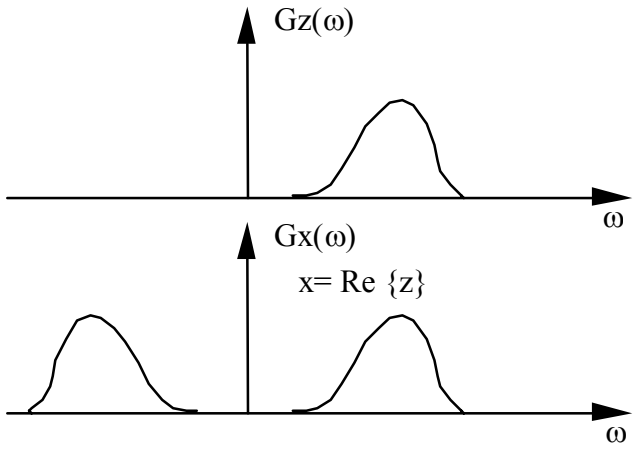

Figure 1. Power spectrum of a complex process z(t) (above), and its real part (below)

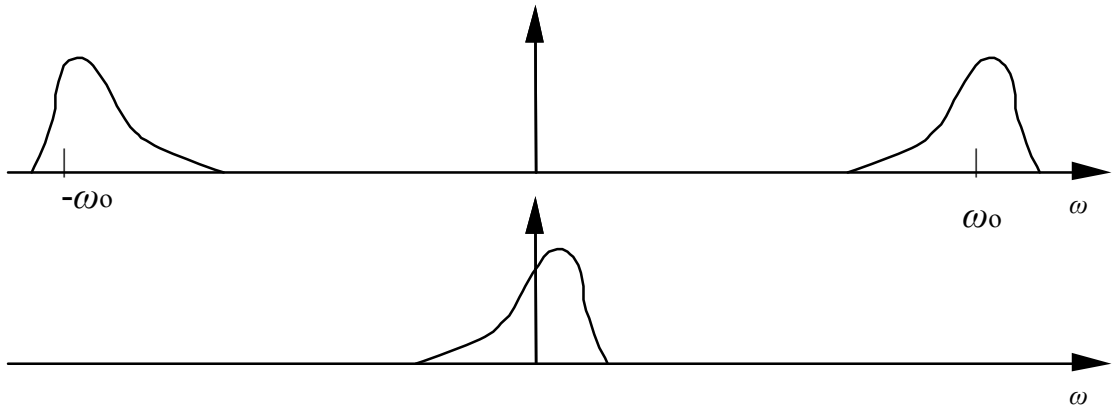

Figure 2. Complex demodulation of a real valued band pass process

Note that the power spectrum is real valued and positive, even though the autocorrelation function is complex valued. The next result shows that the complex Doppler signal satisfies the definition for a complex Gaussian process.

Result 1. The quadrature components of a (real valued) Gaussian band pass signal form a zero-mean complex Gaussian process.

The proof of this result may be found in [1, p 578]. For time discrete signals *z(k), k = -∞,..-1,0,1,..,+∞* , the power spectrum *G(ω)* has the form of a Fourier series in the interval $-\pi < \omega < \pi$, with the autocorrelation function *R(m)* as Fourier coefficients

$$G(\omega) = \sum_m R(m) e^{-i\omega m}$$

$$R(m) = \frac{1}{2\pi} \int_{-\pi}^{\pi} d\omega G(\omega) e^{i\omega m} \qquad (10)$$

An approximation to the power spectrum can be calculated by truncating the Fourier series after lag *m= N*. The resulting approximation to a square formed spectrum is shown in Figure 3

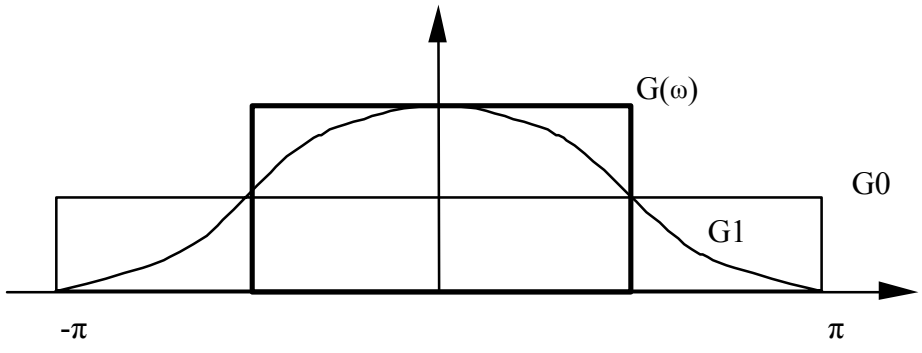

Figure 3. Truncated Fourier series expansion of the power spectrum G(ω) on the interval [-π,π]

B. Estimate of the autocorrelation function

An estimator is a function of random variables which expresses a stochastic property of these variables.

Example 1.

$$z_N = \frac{1}{N}\sum_{k=1}^{N} z(k)$$

$$R_N(m) = \frac{1}{N}\sum_{k=1}^{N} z(k+m)z(k)^* \qquad (11)$$

The complex valued functions z_N and $R_N(m)$ are estimators of the mean value and autocorrelation function for the random process $z(k)$.

A general estimator $f(x_1,...,x_N)$ is a random variable with probability density function determined by the joint probability distribution of $(x_1,...,x_N)$. If the function f is non-linear, the probability density may have a non-Gaussian form, even though the variables $(x_1,...,x_N)$ are jointly Gaussian distributed.

Example 2. The estimator $y = x^2$ has a χ^2 distribution with one degree of freedom, when the random variable x is Gaussian

The quality of an estimator is usually described by two properties

1. Bias is the difference between the expectation value and the correct value.

2. Variance is the second moment of the random variable.

$var\ (f) = < |f - <f>|^2 >$

The estimators z_N and $R_N(m)$ from example 1 are both unbiased (this follows directly from the definition). Note that the autocorrelation estimate $R_N(m)$ is a non-linear, complex valued function of the signal samples $z(n)$, and is therefore not necessarily a Gaussian variable. The probability distribution of $R_N(m)$ with m=1 for three different power spectra are shown in Figure 5. The scatter plots are obtained by computer simulations, and indicate that the probability distribution deviates significantly from a Gaussian distribution.

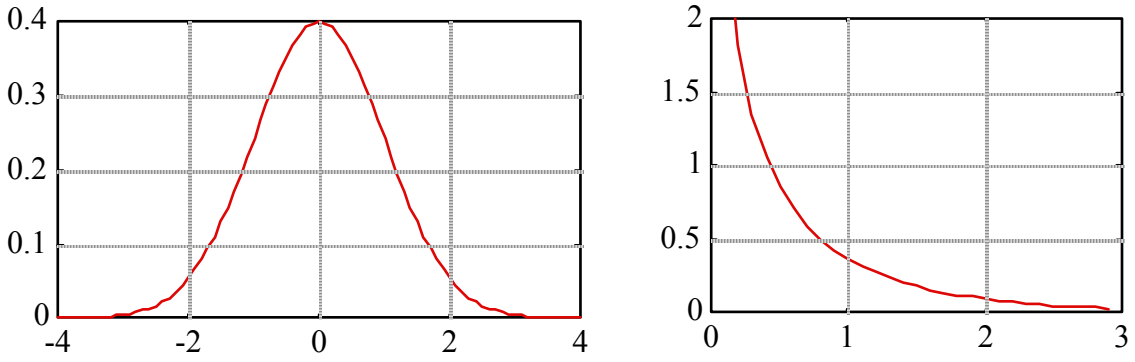

$$p(x) = \frac{1}{\sqrt{2\pi}} e^{-\frac{1}{2}x^2} \qquad p(y = x^2) = \frac{1}{\sqrt{y}} e^{-y}$$

Figure 4. The probability density function of a Gaussian variable x, to the left, and the estimator $f(x)=x^2$, to the right

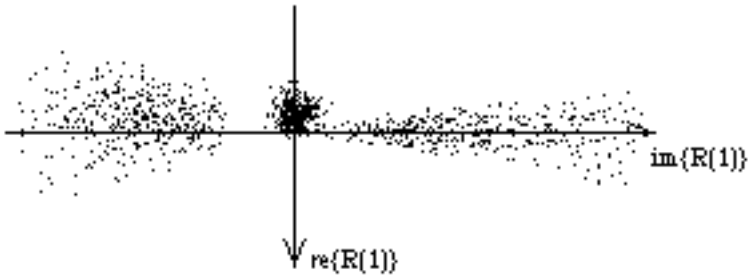

Figure 5. Scatter diagram of the autocorrelation estimator with lag m=1 for three different signals. To the right, a narrow band signal with center frequency $\omega_1 = \pi/2$ to the left, a slightly more broadband signal with $\omega_1 = 3\pi/2$, and in the middle, high-pass filtered white noise.

In order to calculate the variance of non-linear estimators for a complex Gaussian process, the following result is needed to express 4th order moments by a sum of 2nd order moments.

Result 2 If the four random variables *z, u, v, w* are complex, have a zero mean and are jointly Gaussian variables, the fourth order moments can be expressed by

$$< z^* u\, v^* w> = <z^* u><v^* w> + <z^* w><v^* u> \tag{12}$$

This result is used here to calculate the variance of the autocorrelation estimate $R_N(m)$ as defined in Equation (11). Note that this estimator is complex valued when $m \neq 0$. The sum of the variance of the real and imaginary part of $R_N(m)$ is

$$< \left|R_N(m) - R(m)\right|^2 >= \frac{1}{N}\sum_{k=-N}^{N}(1-\frac{|k|}{N})\left|R(k)\right|^2 \tag{13}$$

The variance expression can be derived by applying Equation (12). Note that the variance of $R_N(m)$ decreases with increasing bandwidth.

C. Estimate of the power spectrum

A finite segment *{z(0),...,z(N-1)}* from the zero mean complex Gaussian process is considered. A power spectrum estimator $G_N(\omega)$ for the process based on these signal samples can be obtained as the square of the Fourier transform of this finite length sequence:

$$G_N(\omega) = \frac{1}{N}\left|Z_N(\omega)\right|^2$$
$$Z_N(\omega) = \sum_{m=0}^{N-1} z(m)e^{-i\omega m} \tag{14}$$

The spectrum estimate $G_N(\omega)$ is often called the *periodogram*. The periodogram can also be expressed as a Fourier transform of an autocorrelation function estimate.

$$G_N(\omega) = \sum_{m=0}^{N-1} R'_N(m)e^{-i\omega m}$$
$$R'_N(m) = \frac{1}{N}\sum_{k=0}^{N-m-1} z(k+m)z(k)^* \tag{15}$$

Note that the autocorrelation estimates $R'_N(m)$ are biased for $m > 0$, in contrast to the estimate $R_N(m)$ given in Equation (11).

If a window function $w_N(m)$ is defined as

$$w_N(m) = \begin{cases} 1 & \text{for m = 0,..., N - 1} \\ 0 & \text{elsewhere} \end{cases} \tag{16}$$

the summation in Equation (14) can be expanded to infinity

$$Z_N(\omega) = \sum_m w_N(m) z(m) e^{-i\omega m} \tag{17}$$

and the expectation value for the spectrum estimate can be written

$$\begin{aligned} &< G_N(\omega) >= \frac{1}{2\pi} \int_{-\pi}^{\pi} d\lambda |W(\lambda)|^2 G(\omega - \lambda) \\ &W(\omega) = \sum_m w_N(m) e^{-i\omega m} \end{aligned} \tag{18}$$

This equation shows that the expectation value of $G_N(\omega)$ is a convolution between the true spectrum and the square of the window Fourier transform $W(\omega)$. This introduces a distortion of the spectrum shape. The function $|W(\omega)|$ is shown in logarithmic scale in Figure 6 to the left. It is composed of a main lobe with width = 2/N centered at $\omega=0$, and side lobes with decreasing height, as $|\omega|$ increases.

In order to reduce the side lobe level, other window function shapes can be used. Generally, a window which decreases smoothly towards the end points will have lower side lobe levels than the rectangular window given in Equation (16). The spectrum estimate with a non-rectangular window is usually called the *modified periodogram*. In Figure 6, the rectangular window frequency response is compared to the Hamming window, which is given by

$$w_N(\omega) = \begin{cases} 1.59\left[0.54 - 0.46\cos\left(\frac{2\pi m}{N}\right)\right] & \text{for m = 0,..., N - 1} \\ 0 & \text{elsewhere} \end{cases} \tag{19}$$

The estimator $Z_N(\omega)$ (17) is a weighted sum of the complex Gaussian variables {z(n)}, and is therefore itself a complex Gaussian variable. The power spectrum estimate

$$G_N(\omega) = |Z_N(\omega)|^2 = re\{Z_N(\omega)\}^2 + im\{Z_N(\omega)\}^2$$

will therefore have a χ^2 probability distribution with two degrees of freedom [2]. This distribution has the property that the variance is equal to the square of the mean value, i.e. the fractional variance equals 1.

In [3] the covariance between the power spectrum estimates $G_N(\omega)$ for two different ω is derived

$$\operatorname{cov}\left(G_N(\omega), G_N(\omega+\Delta)\right) = \left| \frac{1}{2\pi N} \int_{-\pi}^{\pi} d\lambda W(\lambda) W^*(\lambda-\Delta) G(\omega-\lambda-\Delta) \right|^2 \tag{20}$$

$$= \begin{cases} < G_N(\omega) >^2 & \text{when } \Delta = 0 \\ 0 & \text{when } |\Delta| > 1/N \end{cases}$$

Note that the fractional variance of $G_N(\omega)$ equals 1, independent of the transform length N, and window form. Since the correlation length of $G_N(\omega)$ is short ($< 1/N$), the variance can be reduced by low pass filtering in the frequency domain.

Another method for reducing the variance of the periodogram is to form an average of periodograms from different segments of the signal. If the segments are non-intersecting, the individual periodograms will be uncorrelated, and the variance will decrease by a factor $1/M$, where M is the number of periodograms which are averaged. For smooth window functions, like the Hamming window, an overlap of 50% will still give a variance reduction factor close to $1/M$ [3].

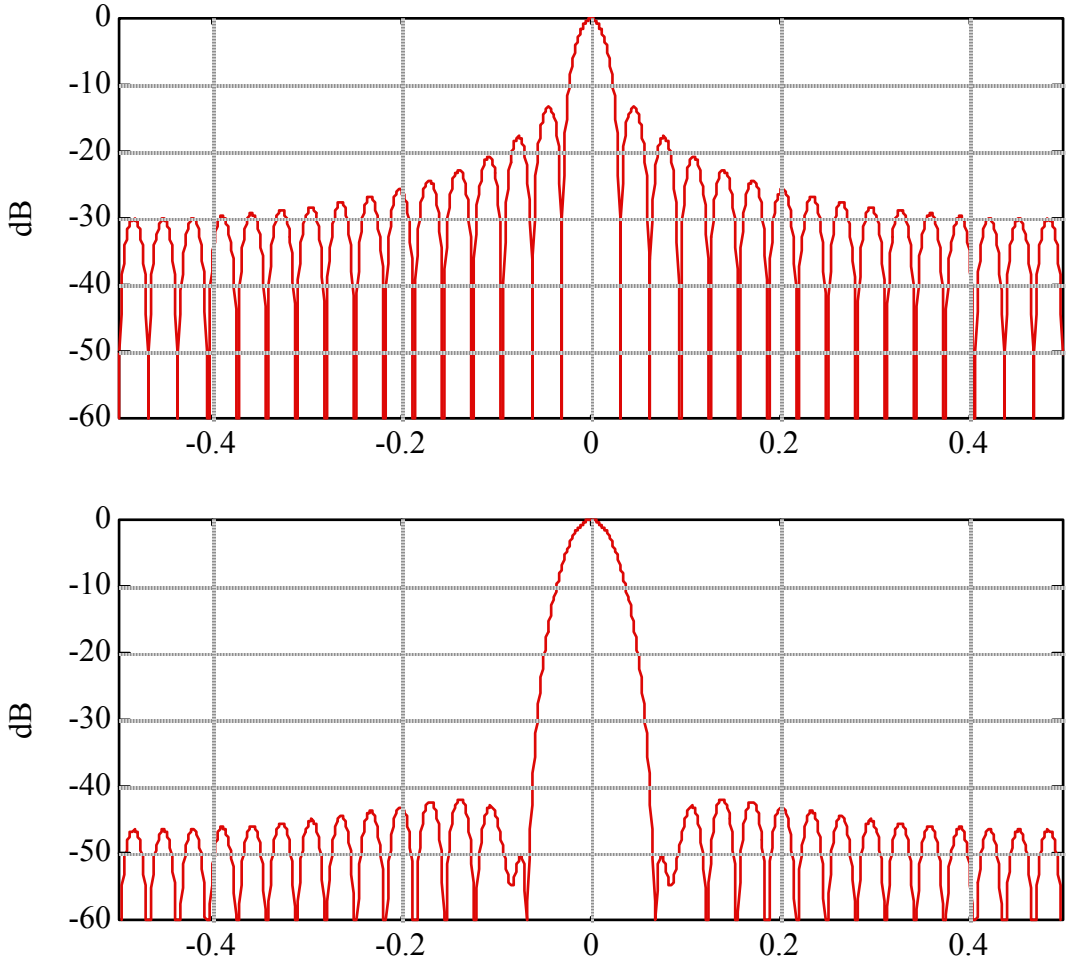

Figure 6. Frequency response of the rectangular window (upper) and the Hamming window (lower) with window length N= 32.

Summary of properties for the power spectrum estimate:

1. Fractional variance = 1 independent of the window form and size
2. $G_N(\omega_1)$ and $G_N(\omega_2)$ are uncorrelated when $|\omega_1-\omega_2| > 1/N$.
3. Increasing window length N gives lower bias, i.e. narrower main lobe, better frequency resolution, but no decrease in variance.
4. Smooth window functions give lower side lobe level, but wider main lobe than are given by rectangular window functions.
5. Decrease in variance can be obtained by averaging spectral estimates from different data segments.

3 Velocity estimators for CW and PW Doppler

A. Velocity information in the Doppler signal spectrum

In Chapter 9 it was demonstrated that the power spectrum of the Doppler signal is completely determined by the blood flow velocity field. Neglecting the transit-time effect, the power spectrum represents a distribution of all radial velocity components in the sample volume. As discussed in Section 9.3, the transit time will increase the width of each frequency component, depending on the relation between the streamline geometry and the ultrasonic beam. True quantitative velocity information is therefore only possible to achieve if *a priori* knowledge on the blood velocity field is added. Some special cases of practical importance are listed below:

1. Uniform velocity field through the whole sample volume. In this case a mean frequency estimator gives the velocity component along the ultrasonic beam.

2. The spatial maximum velocity appears as the velocity component with highest frequency in the Doppler spectrum, provided that the transit time through the Doppler sample volume is sufficiently long. In this case a velocity time sonogram display will show the time waveform of the maximum velocity as the *spectrum envelope* (see Figure 7).

In addition, more qualitative information can be extracted from the Doppler spectrum:

3. Signal power (after high pass filtering) above the noise level indicates that there is moving blood inside the sample volume.

4. Spectral density in the maximum frequency part of the spectrum is related to the volume of blood moving with high velocity. This gives a qualitative measurement of the severity of a high velocity leakage jet.

These examples show that blood velocity information with practical, clinical importance can be deduced from the Doppler spectrum. This chapter deals with methods to estimate this Doppler spectrum with optimum quality.

B. Spectrum sonogram display

In clinical applications of Doppler ultrasound, the periodogram is calculated in real time on a time/frequency grid, and shown in a gray scale display with time along the horizontal axis, and frequency (or velocity) along the vertical axis. This representation of the Doppler signal is often referred to as a velocity time sonogram, or velocity time spectrum. The gray-level is usually a monotone function of the spectrum value in each point. This transfer function can be adjusted to enhance weak spectral components, like in Figure 7.

The spectrum in Figure 7 is generated by a blood flow with different velocities along the ultrasonic beam. The most important clinical information is the maximum Doppler shift, which corresponds to the spatial maximum in the velocity field.

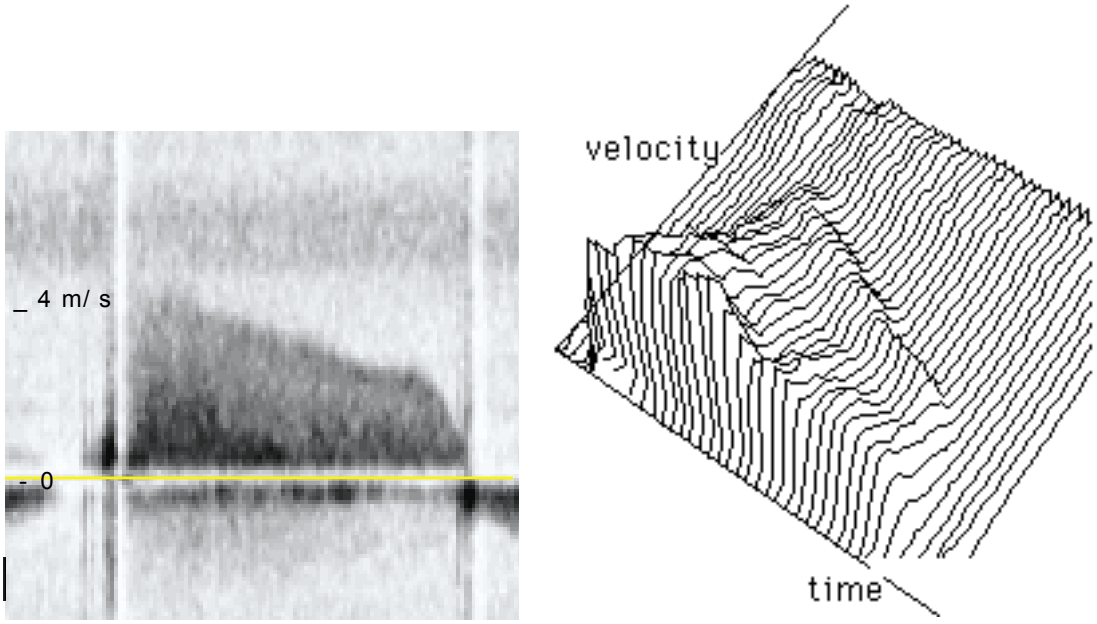

Figure 7. Spectrum sonogram of continuous wave Doppler measurement in a mitral valve stenosis. The peak spectrum envelope exceeds 4 m/sec.

When the ultrasonic beam is directed along a jet stream, the maximum Doppler shift gives the central velocity in the jet, which is related to the pressure drop along the blood stream line. The maximum Doppler shift as a function of time is often called the *spectrum envelope* , and can be delineated from the spectrum sonogram, even if the spectral signal-to-noise ratio is low. The bias of the periodogram has little influence on the spectral envelope.

When strong signal components are present, the side lobes from the strong components may interfere with the weaker components near the spectral envelope. In this case, a smooth window function with a low side lobe level is preferred. In Figure 8 the difference between a rectangular and a Hamming window is demonstrated in a signal with a strong low frequency component.

The Doppler signals from blood flow in the heart and arteries are highly non-stationary, due to the variation of the blood velocity through the heart cycle. Especially in the early part of the systole, the acceleration is high. This limits the ability to use long transform lengths and/or temporal smoothing to reduce estimator variance.

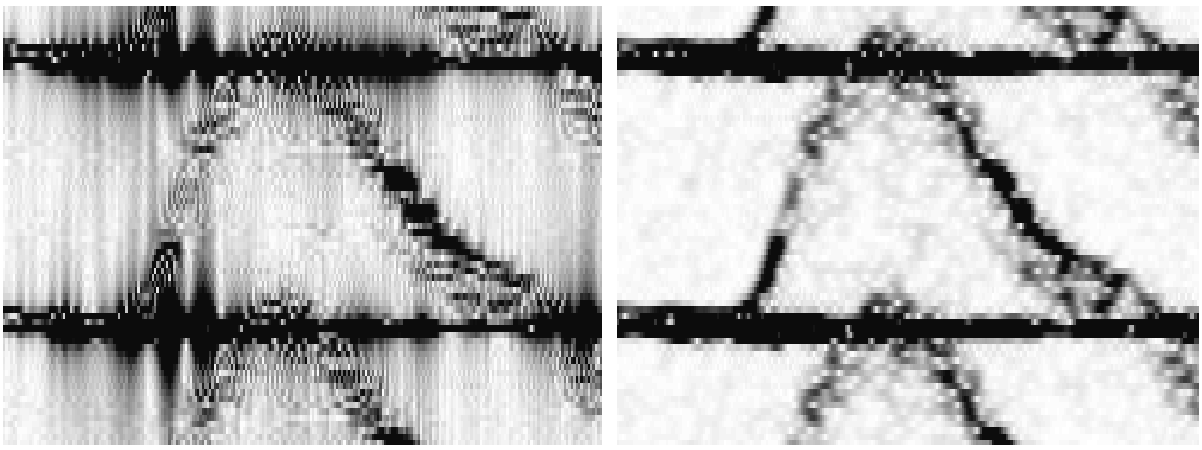

Figure 8. Difference in the spectral dynamic range between the rectangular window (to the left) and the Hamming window (to the right)

The benefit of using a high degree of overlap between the transforms is demonstrated in Figure 9 and 10, which shows the signal waveform and the spectrum with different degrees of overlap. The trade-off between frequency resolution and temporal resolution in spectrum sonogram is shown in Figure 11, where the same data is shown with four different window lengths.

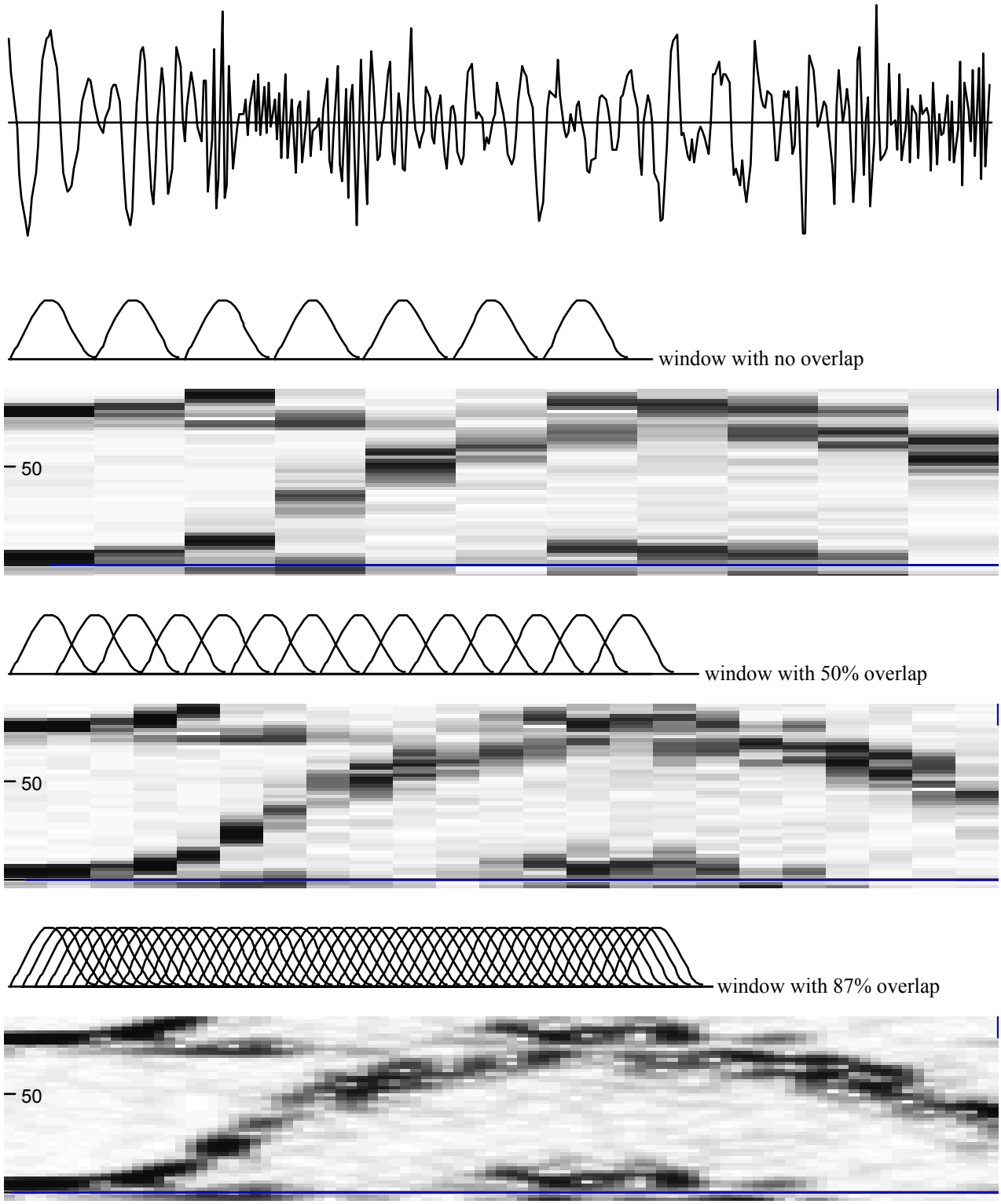

Figure 9. Spectrum analysis of a non-stationary signal with different degrees of overlap. The upper plot is the signal waveform; the window positions are indicated for each spectral line in the lower sonogram displays.

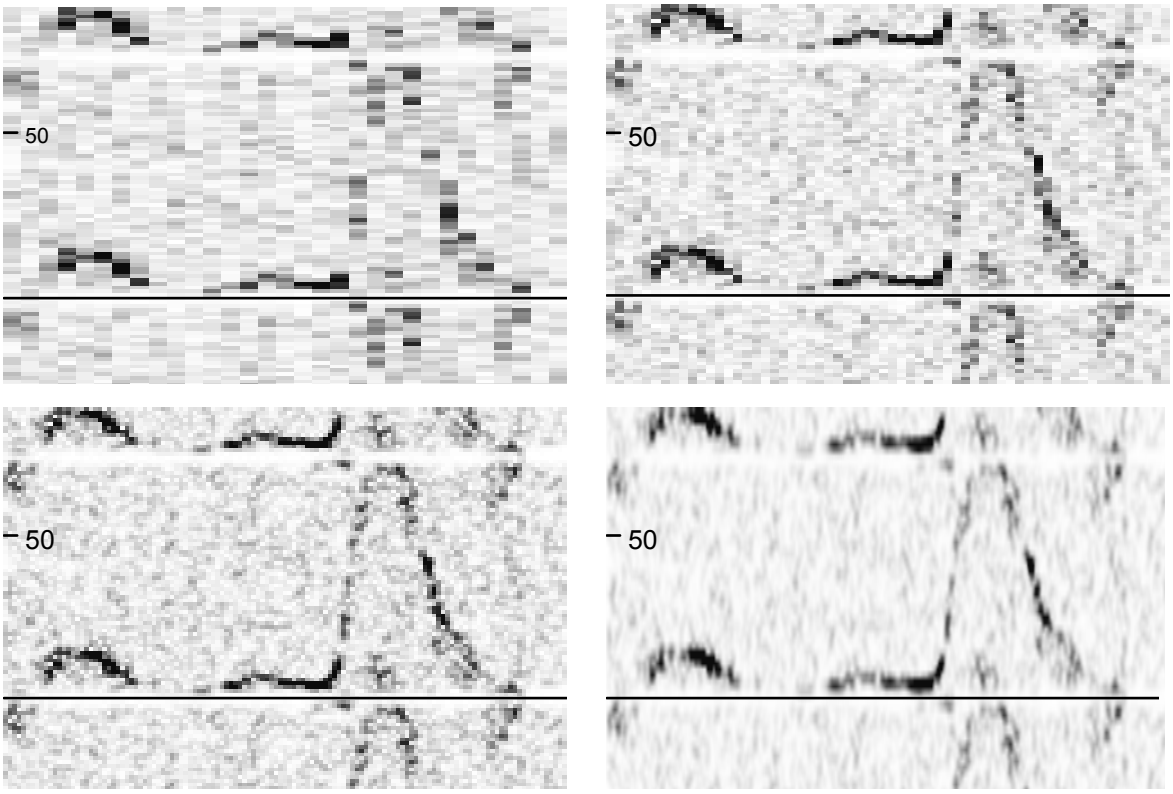

Figure The Doppler signal in white noise analyzed with different degrees of window overlap. Upper left is without overlap, upper right is with 50% overlap, lower left is with 75% overlap. No smoothing has been performed on these samples. Lower right is with 4 point smoothing. It is a 64 point Hamming window.

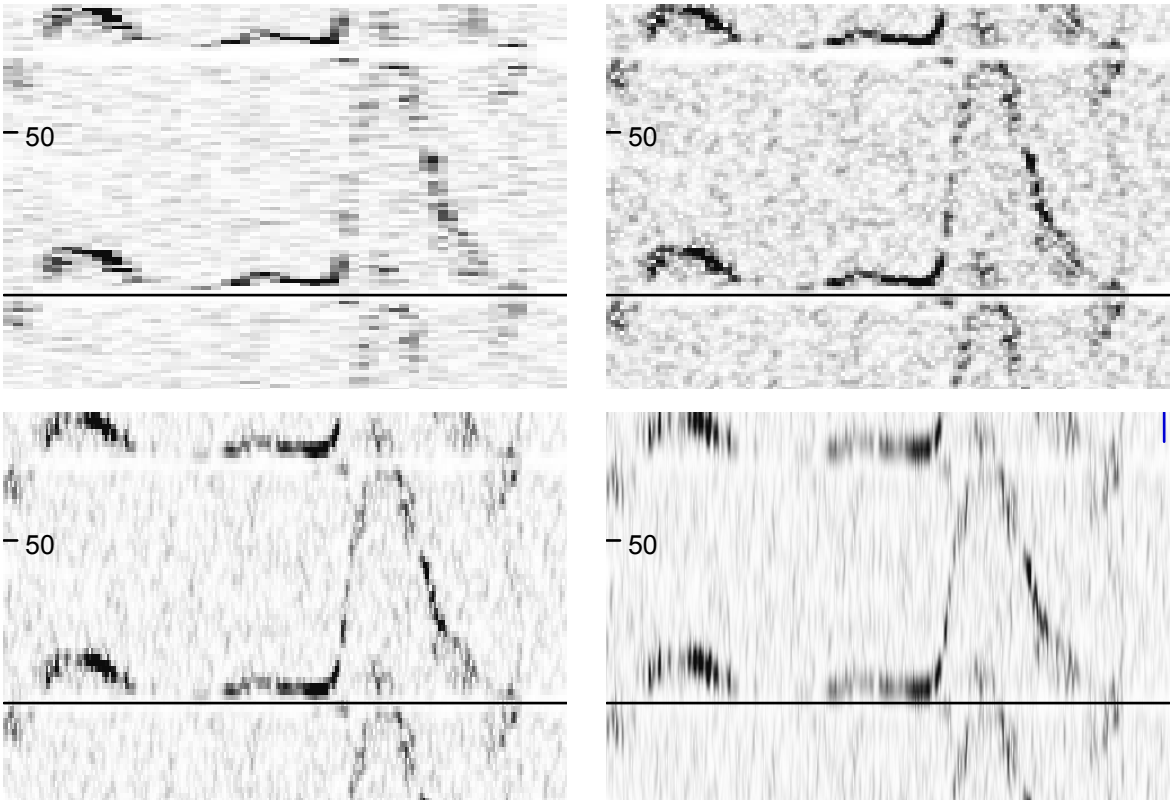

Figure 11. The performance of the spectrum sonogram as a function of window length. Upper left: 150 points, upper right: 64 points, lower left: 32 points, and lower right: 16 points. The window type is Hamming and the degree of overlap is 75% in all pictures.

D. Wall motion rejection

Signals from stationary and slowly moving targets like vessel walls and other tissue structures give an additive low frequency noise (also called clutter noise) which usually is much stronger than the signal from blood. The signal-to-clutter level can be as low as -100 dB [ref] for CW Doppler, 2 MHz ultrasound frequency, but is usually better in PW Doppler, and for higher frequency. Clutter signals are usually suppressed in a high pass filter stage, which is designed with sufficient stop-band damping to minimize the error in the velocity parameter estimator. If a mean frequency estimator is used for blood velocity estimation, the low frequency clutter signal will give a bias towards zero according to

$$\textit{Fractional bias} = P_{cl} / (P_{cl}+P_b) \tag{24}$$

where P_{cl} and P_b are the signal power from clutter and blood, respectively. In order to keep the fractional bias below 10%, the signal to clutter level after the high pass filter must be at least +10 dB. For spectrum analysis, a higher clutter level can be accepted, since the different frequency components are separated in the spectral display. However, when the side lobes from clutter signals exceed the receiver noise level, this can be misinterpreted as blood flow signal. For a Hamming window of length N, the spectral density of the side lobes equals the receiver noise level when the noise-to-clutter level equals

$$\text{Noise-to-clutter level} = 10 \log(N/2) - 40 \quad [dB] \tag{25}$$

For window length N= 64, a signal-to-clutter level after the high pass filter equal to -25 dB will satisfy this requirement.

A stop-band requirement of 75-110 dB for the high pass filter means that the filter must have a relatively long impulse response. However, short transition signals from opening and closing of heart valves may in this case cause ringing in the filters.

4 Visualization of 2D Doppler signals

A. Spectral parameters for characterizing blood-flow

Visualization of 2D Doppler signals is usually done in combination with ultrasound echo imaging, as a color-coded overlay to the gray scale tissue image. This modality is therefore called color flow mapping, or color flow imaging. In color flow imaging, the object is to extract information related to the velocity field as reflected in the power spectrum of the Doppler signal at each point of the 2D sector. Compared to conventional Doppler (i.e. CW and PW Doppler technique), the ability to present quantitative velocity information is limited due to

1. Limited information content in the signal, i.e. short observation time, low signal-to-noise ratio, and low Nyquist velocity limit.

2. Insufficient signal processing/display. Full spectrum analysis in each point of the sector is difficult to visualize.

The advantage of color flow imaging, compared to conventional Doppler, lies in the ability to show the spatial distribution of blood-flow, and thereby localize abnormal flow patterns. In order to present 2D Doppler in one image, all velocity information from each range cell must be compressed into one color value. Usually, three spectral parameters are

estimated and combined in a color coding scheme: the signal power, bandwidth, and mean frequency.

An example which shows how these parameters describe the blood flow in a section of the human heart is shown in Figure 14. The Doppler spectrum, signal power, bandwidth, and mean frequency are plotted when the ultrasonic beam is swept over a region with different velocity patterns. The drawing is a section of the left ventricle in the expansion phase, with the blood flow indicated by stream lines. The filling of the ventricle gives moderate blood velocities upwards at point D, and downwards at point B. At point C, a high velocity jet stream enters the ventricle from a leaking aortic valve. The Doppler signal power has low values in region A, and E, which is outside the blood vessel, and high value in region B, C and D. This parameter is used to determine whether blood is present in the sample volume. The laminar flow in region B and D give low bandwidth, and good quality mean frequency estimate which can be used to measure the actual velocity in each point. In region C high velocities and turbulence give a high bandwidth signal. Here the mean frequency gives no information on the actual blood velocity.

The spectral parameters signal power, mean frequency, and square bandwidth can be defined as the zero, first, and second order central moments of the power spectrum G(ω):

Signal power: $$P = \int_{-\pi}^{\pi} d\omega G(\omega)$$

Mean frequency: $$\omega_1 = \frac{1}{P}\int_{-\pi}^{\pi} d\omega \omega G(\omega)$$

Bandwidth: $$B = \sqrt{\frac{1}{P}\int_{-\pi}^{\pi} d\omega (\omega - \omega_1)^2 G(\omega)} \qquad (26)$$

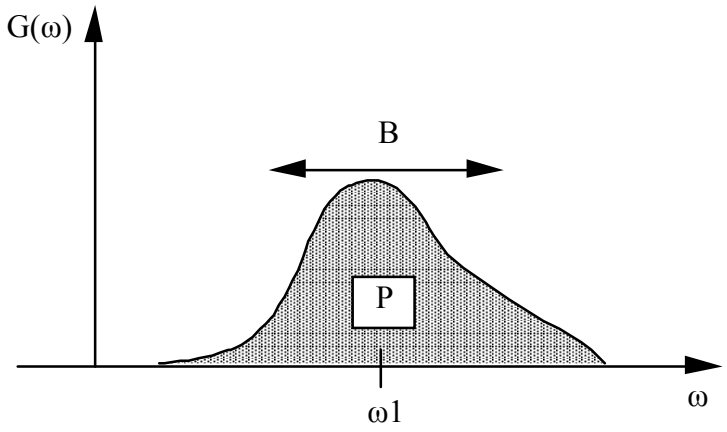

Figure 15. Signal power P, mean frequency ω1 and bandwidth B of the Doppler spectrum.

Spectral parameter estimators can be divided into two groups:

1. Frequency domain estimators. These are obtained by substituting a full spectrum estimate into the definition Equation (26).

2. Time domain estimators. These are obtained directly from the signal samples, or the autocorrelation estimate.

Frequency domain estimators have the advantage that unwanted signal components (like white thermal noise, and low frequency wall motion signals) can be subtracted from the spectrum estimate before calculating the actual parameters. Time domain estimators have the advantage of simplicity, which makes them suitable for real-time implementation. In the following, estimators for signal power, mean frequency, and bandwidth will be analyzed.

Signal power estimator

An estimator for the signal power P = R(0) can be obtained by setting the lag m=0 in the autocorrelation estimate defined in Section 2. The bias and variance of this signal power estimator is found from Equation (13):

$$P_N = R_N(0) = \frac{1}{N}\sum_{k=1}^{N}|z(k)|^2$$

$$Bias(P_N) = 0$$

$$Var(P_N) = \frac{1}{N}\sum_{k=-N}^{N}\left(1-\frac{|k|}{N}\right)|R(k)|^2 \approx \int_{-\pi}^{\pi} d\omega G(\omega)^2 \approx \frac{P^2}{BN} \qquad (27)$$

The first approximation is valid for large N, and the second approximation shows the dependency on the bandwidth B. Note that the variance of P_N decreases with increasing bandwidth B.

Mean frequency estimator

The autocorrelation function with lag *m=1* can be expressed as an integral over ω of the complex exponential *exp(iω),* weighted by the power spectrum *G(ω),* Equation (10)

$$R(1) = \frac{1}{2\pi}\int_{-\pi}^{\pi} d\omega G(\omega) e^{i\omega} \qquad (28)$$

In Figure 16 the power spectrum *G(ω)* is displayed as a polar plot, demonstrating that the complex number *R(1)* represents the center of gravity of the trace $\{G(\omega)exp(i\,\omega);\ -\pi < \omega < \pi\}$ in the polar diagram. The phase of *R(1)* will therefore be an approximation of the mean frequency, as defined in Equation(26). This can be verified by a power series expansion of *exp(i ω)* in the point $\omega_1 = phase(R(1))$.

$$
\begin{aligned}
R(1) &= e^{i\omega_1}\int_{-\pi}^{\pi} d\omega G(\omega) e^{i(\omega-\omega_1)} \\
&= e^{i\omega_1}\int_{-\pi}^{\pi} d\omega G(\omega)\{1+i(\omega-\omega_1)-\frac{1}{2}(\omega-\omega_1)^2+....\} \\
&\approx Pe^{i\omega_1}\{1-\frac{1}{2}B^2\}
\end{aligned}
$$

$$
B^2 = \frac{1}{P}\int_{-\pi}^{\pi} d\omega(\omega-\omega_1)^2 G(\omega) \tag{29}
$$

The last approximation is valid when G(ω) vanishes outside a small interval around $\omega=\omega_1$. P is the signal power, and B is the RMS-bandwidth.

A mean frequency estimator is obtained by using the autocorrelation estimator $R_N(1)$, with m=1.

$$
\omega_{1N} = phase(R_N(1)) = \arctan\left(\frac{\mathrm{Im}\{R_N(1)\}}{\mathrm{Re}\{R_N(1)\}}\right)
$$

$$
R_N = \frac{1}{N}\sum_{k=1}^{N} z(k+1)z(k)^* \tag{30}
$$

For narrow band signals and large *N*, the estimator bias ≈ 0, and the variance is approximately given by

$$
Var(\omega_{1N}) \approx \frac{B^2}{N} \tag{31}
$$

Note that the variance increases with increasing bandwidth B, in contrast to the variance of the signal power estimate, which decreases with increasing bandwidth.

Bandwidth estimator

$$
B_N = \sqrt{2}\sqrt{1-\frac{|R_N(1)|}{R_N(0)}} \tag{32}
$$

For white noise, corresponding to *|R(1)| = 0*, the RMS bandwidth *B=π/sqrt(3)*=1.84. Using (32) gives the value *sqrt(2)* which is 30% too low.

In Figure 17, the expectation value and variance for the normalized autocorrelation function estimator are indicated in the complex plane for two different signals, one with narrow bandwidth, and one with broad bandwidth.

The normalized autocorrelation function is defined as

$$
\rho(m) = \frac{R(m)}{R(0)} \tag{33}
$$

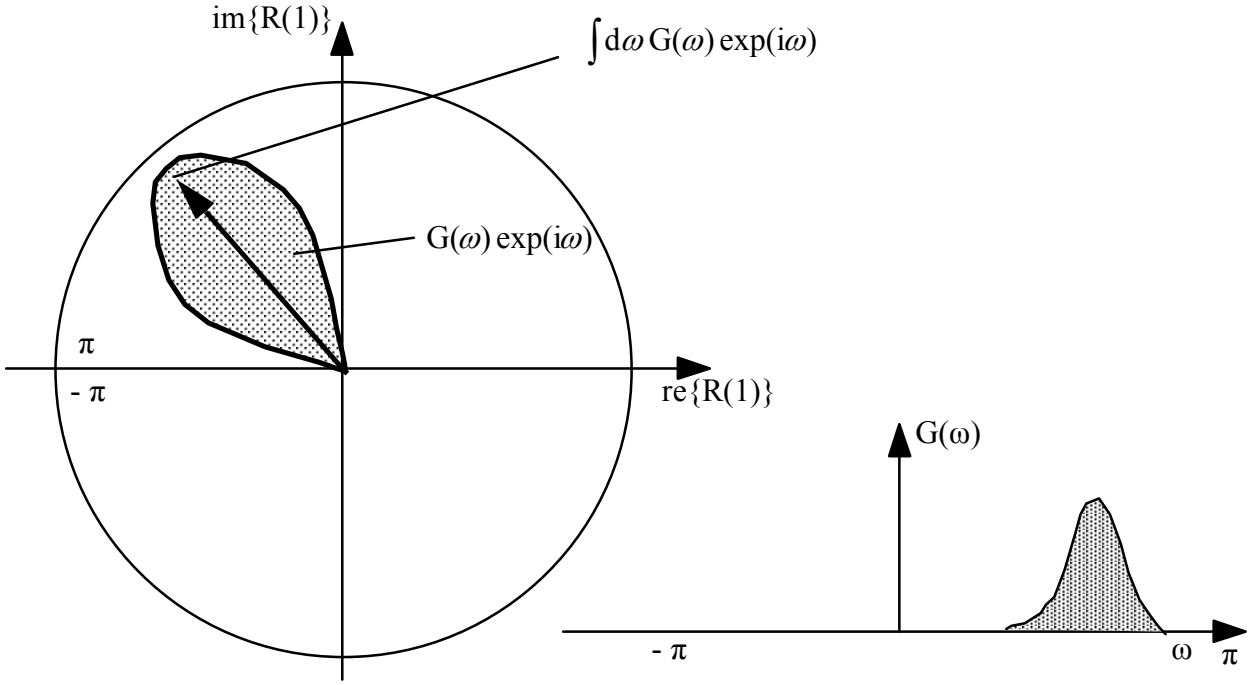

Figure 16. Power spectrum G(ω) to the right, and its polar presentation and the complex autocorrelation R(1) to the left.

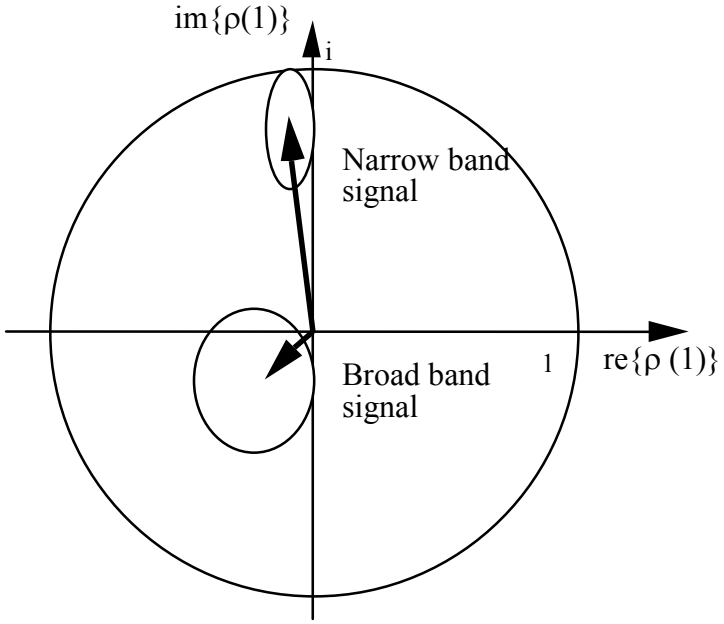

Figure 17. The estimate of the normalized autocorrelation function ρ(1) for two different signals. Expectation values are indicated by the arrows, and distribution around the mean values are indicated by ellipses.

From Equation (29) the following relation between the absolute value $|R(1)|$ and the bandwidth parameter B is valid, when the bandwidth is low:

$$|\rho(1)| = \left|\frac{R(1)}{P}\right| \approx 1 - \frac{1}{2}B^2 \tag{34}$$

By inverting Equation (34), and inserting the autocorrelation estimate for *R(1)* and *R(0),* a bandwidth estimator is obtained.

B. Wall motion rejection for 2D Doppler

The first multi-gated Doppler used a separate signal processing unit for each depth which made the equipment quite complex. To obtain cost effective signal processing, much work was done in the late seventies and early eighties based on the use of one signal processing unit for all depths. This is called **serial signal processing** since the back-scattered signals from deeper depths arrive in series for each range cell. The processing unit operates on the signal as it returns, to generate a velocity estimate from each range.

The first experiments with serial processing were presented in 1975 using the **moving target indicator (MTI)** technique, that was previously developed for radar and sonar systems. In the simplest form of this technique, the back-scattered signals from two consecutive ultrasound pulses are subtracted so that the signals from targets that do not move are removed as illustrated in Figure 26b. This is called **fixed target canceller (FTC)**. For peripheral vessels where the tissue structures are moving slowly, this method removes the signals from the tissue so that we are left with the signals from the blood, which are moving targets (hence the name MTI). The blood velocity profile along the beam is then estimated from the Doppler frequency.

The FTC is the same as the high pass filter for the PW/CW Doppler as described in Section 2.6B. It removes the low Doppler frequencies from the tissues that move slowly and allows the high Doppler frequencies from the blood which moves faster to pass through. We therefore use the term FTC and high pass filter interchangeably.

For cardiac examination, the simple fixed target canceller in Figure 26 is not adequate for removing the tissue signals, since the cardiac walls are moving rapidly (~ 20 cm/sec) and produce quite large Doppler shifts. For this reason, a considerable amount of wall motion was present in the first color flow mappers. What is needed for the heart is a **slow target canceller (STC)** rather than a fixed target canceller. STC's which compare the signals from several consecutive ultrasound pulses have been designed to solve this problem. In Figure 27 the frequency response for the simple fixed target canceller is compared with a higher order Butterworth filter.

However, one frequently notes that wall motion artifacts are still a problem in many color flow imaging systems. Thus, for cardiac examination, the STC is one of the most critical components of the instrument for good quality color flow imaging, and thus requires highly advanced design. We review some aspects of STC's below.

Let *x(n)* be the complex envelope of the Doppler signal from pulse n, sampled at a constant depth range. The STC output signal *y(k)* at time sample k is then formed as a combination of x(n) from several pulses. With the continuous beam sweep as with mechanical scanning we have a long sequence of the input signal *x(n)* for input to the STC filter.

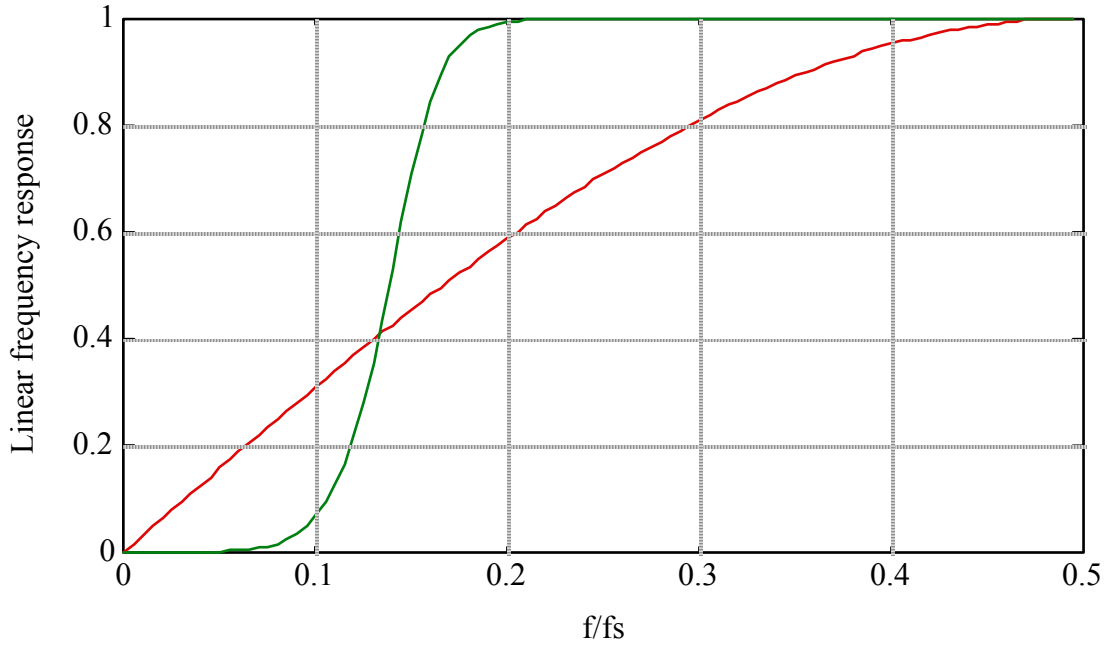

Figure 27. Frequency response of the simple FTC compared with a 6 order Butterworth high pass filter.

A standard linear time invariant filter of the type

$$y(k) = \sum_n h(n)x(k-n) \tag{37}$$

is then often used. The filter impulse response is *h(n)*, which can be both of the IIR (infinite impulse response) and the FIR (finite impulse response) type. The filter is designed as a standard high pass filter that attenuates the low frequency Doppler shifts from the tissue.

With electronic scanning, the beam direction is stepped in discrete directions, while transmitting several pulses for each direction. This produces a finite number of signal samples (x(1),..., x(N)) for each beam direction. Using the time invariant filter, we will get a settling time of the filter for each new beam direction, as illustrated in Figure 28. This can partly be avoided by using a time variant filter, where the impulse response is different for each sample of the output signal. The filter should however be linear, in order to avoid inter-modulation between the tissue signal and the blood signal. Since the filter is linear, it can be described mathematically as a linear transform on the N dimensional complex vector space $\boldsymbol{C}^N$, and can therefore be performed by multiplying the input vector with a *NxN* transformation matrix $A = \{a(n,m)\}$

$$\begin{aligned} &\textit{Input vector: } \underline{x} = (x(1),\ldots,x(N)) \\ &\textit{Output vector: } \underline{y} = (y(1),\ldots,y(N)) = A\underline{x} \end{aligned} \tag{38}$$

$$y(k) = \sum_{n=1}^{N} a(n,k)x(n) \;;\; k = 1,..,N$$

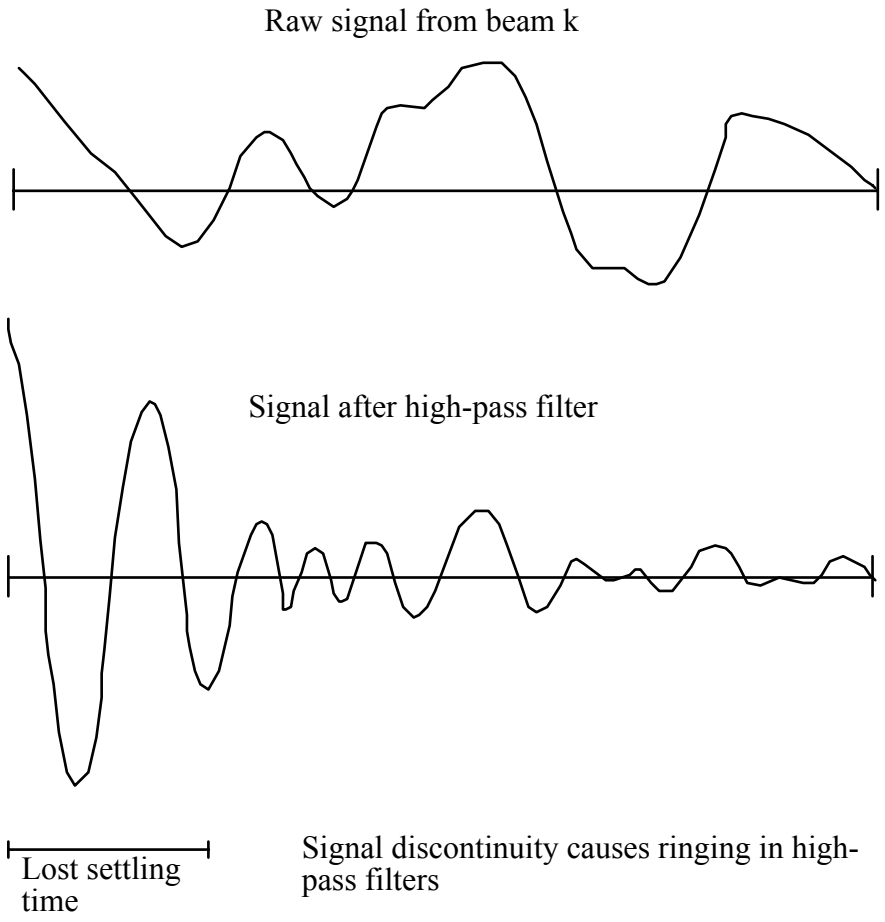

Figure 28. The settling time of the high pass filter for a phased array scanner.

A time invariant FIR filter with an impulse response *h(n), n=0,1,..,M* has a filter matrix given by:

$$a(n,k) = \begin{cases} h(k-n) & for \;\; k \geq n \;\; and \;\; k > M \\ 0 & elsewhere \end{cases} \tag{39}$$

Note that the first M samples in the output signal is zero. The frequency response of the FIR filter can be defined by the Fourier transform of the impulse response h(n). This definition of the frequency response can not be applied to the general linear filter. However, a frequency response function *Ho(ω)* can be defined as the power of the output signal when the input is a complex harmonic signal.

$$\begin{aligned} x(k) &= e^{ik\omega} \qquad ; \; k = 1, 2, .., N \\ y(k) &= \sum_{n=1}^{N} a(n,k) e^{in\omega} \equiv A_k(\omega) \\ H_0(\omega) &\equiv \tfrac{1}{N} \sum_{k=1}^{N} |y_\omega(k)|^2 = \tfrac{1}{N} \sum_{k=1}^{N} |A_k(\omega)|^2 \end{aligned} \tag{40}$$

The quantity $A_k(\omega)$ is the Fourier transform of row number k in the filter matrix. Since the transform is linear, a constant phase shift of the input signal will give a factor $e^{i\omega}$ with unit length, and will therefore not influence the output power. This means that the frequency response in (40) is well defined. This is a unique property for complex base band signals.

For real valued signals, an ensemble average over all possible phases of the input signal is necessarily in order to obtain a well defined frequency response [4]. In the complex case, the power of the real- and imaginary parts both varies with the phase of the input signal in such a way that the sum is constant. Note that for FIR filters, the frequency response defined in (40) coincide with the usual definition.

If the filter matrix elements attain complex values, non-symmetric frequency responses can be obtained, which is useful for adaptive clutter filters, where the Doppler shift of the tissue signal is estimated from the signal.

Unlike the linear convolution filter, the output will not in general be a complex harmonic sequence, but may contain frequency components which are not present in the input signal. This property can cause severe problems in color flow imaging, where strong clutter signals may generate higher frequency components which affect both the center frequency and the bandwidth estimate. This frequency distortion is only absent for FIR-filters, where the number of non-zero output samples must be reduced to N-M, where M is the FIR filter order. A reduction of the number of output samples will increase the variance in the velocity parameter estimates, and should therefore be minimized. Several methods have been proposed for reducing the "ring-down time" in the filter [10]. The basic idea is to extend the signal interval by some sort of prediction, followed by a FIR or IIR convolution filter. As long as the predicted values are formed by linear combinations of the original input signal, the total filter operation will still be linear, and can therefore be performed by a matrix multiplication.

Another approach was taken by Hoeks et. al [4], where the clutter signal was estimated by a least square fitting to a straight line, and then subtracted from the input signal. This is one example from a class of filters which is called *regression filters.* If we assume that the clutter signal is contained in a subspace κ of $\boldsymbol{C}^N$, the projection transform P_κ from $\boldsymbol{C}^N$ into κ gives the least square fit to the clutter component. The clutter filter will then have the form $A = I - P_\kappa$, which is a projection into the orthogonal complement of κ

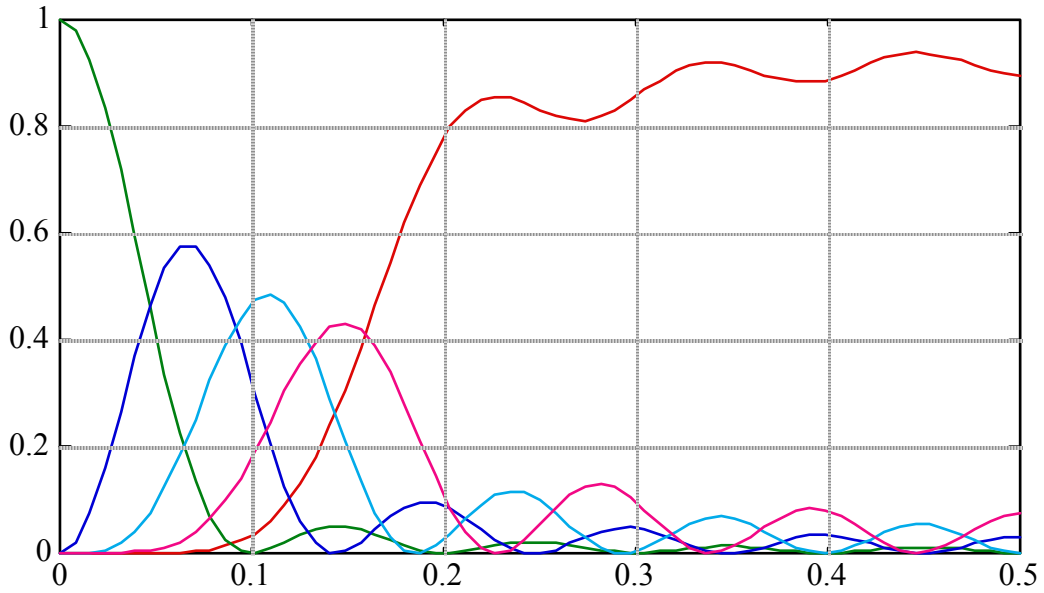

Fig. 29 Frequency spectra for the Legendre polynomials, $|B_p|$™ for p=0, 1, 2, 3, and the frequency response for the 3rd order polynomial regression filter. N=10.

If *{b,, b/,...,bP}* is an orthonormal basis for *κ*, the filter operation can be performed by calculating the projection along each basis vector, and subtract the projections from the original signal. The filter matrix *{a(n,m)}* and the frequency transfer function for the regression filter get the following form:

$$a(n,m) = \delta(n-m) - \sum_{p=0}^{P} b_p(n)^* b_p(m)$$

$$H_0(\omega) = 1 - \tfrac{1}{P+1} \sum_{p=0}^{P} \left| B_p(\omega) \right|^2 \qquad (41)$$

$$B_p(\omega) \equiv \sum_{n=1}^{N} b_p(n) e^{in\omega}$$

The Legendre polynomials form a set of basis functions which is suitable for clutter rejection filters. The Legendre polynomials can be obtained by applying the Gram-Schmidth orthonormalization process to the series of polynomials *{1, n, n2,...,n^P}*. In Fig. 29 the frequency responses for the polynomial basis functions are shown, for *N=10*, and *p=0,1,2,3*. The corresponding clutter rejection filter is equivalent to a least square polynomial fit of order *P* to the clutter component. Note that the basis functions are real valued, giving a symmetric frequency response. Fig. 30 shows the frequency responses for the polynomial projection filter, for different order *P*.

Further reading: see [9, 10, 11]

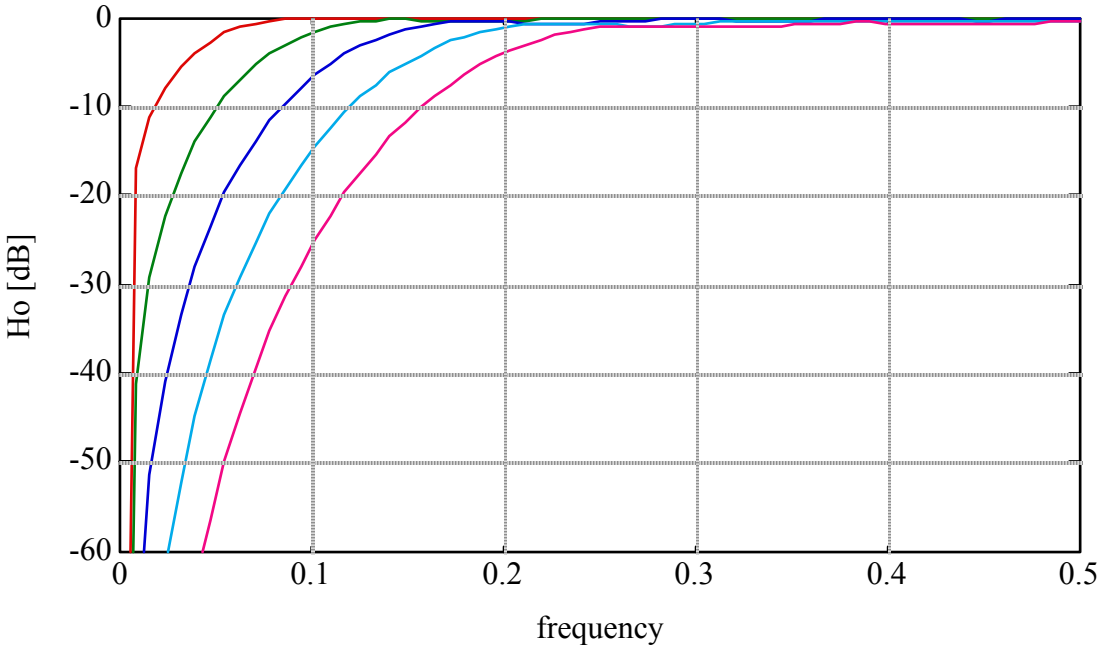

Figure 30. Frequency response for the Legendre polynomial regression filter, with order P=0, 1, 2, 3, and 4. N=10.

7 References

[1] H. L. van Trees, *Detection, Estimation, and Modulation theory, Part III*: John Wiley & Sons, New York, 1971.

[2] M. B. Priestly, *Spectral Analysis and Time Series*. London: Academic Press, 1981.

[3] K. Kristoffersen, "Real time spectrum analysis in Doppler ultrasound blood velocity measurement," SINTEF report Nov. 1984.

[4] H. Torp, "Signal processing in realtime, two dimensional Doppler color flow mapping," : University of Trondheim, Norway, 1991.

[5] H. L. van Trees, *Detection, estimation, and modulation theory. Part I*,: John Wiley & Sons, New York, 1968.

[6] L. S. Wilson, "Description of Broadband Pulsed Doppler Ultrasonic Processing using the Two-Dimensional Fourier Transform," *Ultrasonic Imaging*, vol. 13, pp. 301 - 315, 1991.

[7] H. Torp, K. Kristoffersen, and B. Angelsen, "Autocorrelation Techniques in Color Flow Imaging. Signal model and statistical properties of the Autocorrelation estimates," *IEEE Trans. on Ultrasonics, Ferroelectrics, and Frequency control*, vol. 41, pp. 604 - 612, 1994.

[8] H. Torp and K. Kristoffersen, "Velocity Matched Spectrum Analysis: A new Method for suppressing Velocity Ambiguity in Doppler Sonogram," *Ultrasound in Medicine and Biology*, vol. 21, no. 7, pp. 937 - 944, 1995.

[9] H. Torp, "Clutter rejection filters in Color Flow Imaging: A theoretical Approach," *IEEE Trans. on Ultrasonics, Ferroelectrics, and Frequency control*, vol. 44, no. 2, pp. 417 - 424, 1996.

[10] A. Kadi and T. Loupas, "On the performance of Regression and step-initialized IIR Clutter filters for color Doppler systems in diagnosing medical ultrasound," *IEEE Trans. on Ultrasonics, Ferroelectrics, and Frequency control*, vol. 42, no. 5, pp. 927 - 937, 1995.

[11] A. P. Hoeks, J. J. van-de-Vorst, A. Dabekaussen, P. J. Brands, and R. S. Reneman, "An efficient algorithm to remove low frequency Doppler signals in digital Doppler systems," *Ultrason Imaging*, vol. 13, no. 2, pp. 135-44, 1991.